Stimulation of Arteriogenesis in Skeletal Muscle by Microbubble Destruction With Ultrasound

Ji Song, Ming Qi, Sanjiv Kaul and Richard J. Price

Circulation 2002;106;1550-1555; originally published online Aug 26, 2002;
DOI: 10.1161/01.CIR.0000028810.33423.95
Circulation is published by the American Heart Association. 7272 Greenville Avenue, Dallas, TX 72514
 Print ISSN: 0009-7322. Online ISSN: 1524-4539

Stimulation of Arteriogenesis in Skeletal Muscle by Microbubble Destruction With Ultrasound

Ji Song, PhD; Ming Qi, BS; Sanjiv Kaul, MD; Richard J. Price, PhD

Background—The application of ultrasound to microbubbles in skeletal muscle creates capillary ruptures. We tested the hypothesis that this bioeffect could be used to stimulate the growth and remodeling of new arterioles via natural repair processes, resulting in an increase in skeletal muscle nutrient blood flow.

Methods and Results—Pulsed ultrasound (1 MHz) was applied to exposed rat gracilis muscle after intravenous microbubble injection. Capillary rupturing was visually verified by the presence of red blood cells in the muscle, and animals were allowed to recover. Ultrasound-microbubble–treated and contralateral sham-treated muscles were harvested 3, 7, 14, and 28 days later. Arterioles were assessed by smooth muscle α-actin staining, and skeletal muscle blood flow was measured with 15-μm fluorescent microspheres. An $\approx$65% increase in arterioles per muscle fiber was noted in treated muscles compared with paired sham-treated control muscles at 7 and 14 days after treatment. This increase in arterioles occurred across all studied diameter ranges at both 7 and 14 days after treatment. Arterioles per muscle fiber in sham-treated and untreated control muscles were comparable, indicating that the surgical intervention itself had no significant effect. Hyperemia nutrient blood flow in treated muscles was increased 57% over that in paired sham-treated control muscles.

Conclusions—Capillary rupturing via microbubble destruction with ultrasound enhances arterioles per muscle fiber, arteriole diameters, and maximum nutrient blood flow in skeletal muscle. This method has the potential to become a clinical tool for stimulating blood flow to organs affected by occlusive vascular disease. **(*Circulation*. 2002;106:1550-1555.)**

Key Words: revascularization ■ microcirculation ■ angiogenesis ■ ultrasonics ■ contrast media

The targeted stimulation of neovascularization as a therapeutic tool for restoring nutrient blood flow (NBF) to organs affected by occlusive vascular disease has been pursued for the past several years. Typically, therapeutic neovascularization is stimulated by the targeted delivery of growth factor genes or proteins to the ischemic region.[1–4] Alternatively, transmyocardial laser revascularization may be used to initiate an inflammatory response, which is hypothesized to subsequently elicit neovascularization.[5–8]

Recently, investigators have begun to test the feasibility of using microbubbles for therapeutic purposes, primarily as targeted gene delivery systems.[9–12] These studies illustrate the promise of ultrasound-microbubble–based therapeutics. We have shown that the application of low-frequency ultrasound to intravascular microbubble contrast agents creates small capillary ruptures in exteriorized rat skeletal muscle[13,14] and that this effect is dependent on applied ultrasound power.[14] A similar result has been recently reported for intact mouse muscle[15] and rabbit myocardium.[16]

Given the abundance of evidence that transmyocardial laser revascularization induces neovascularization via wound-healing responses,[5–8] we hypothesized that these small capillary ruptures could elicit neovascularization through a similar wound-healing mechanism. In the present study, we were particularly interested in determining whether the formation and remodeling of arterioles, the process denoted as arteriogenesis, occurs with this treatment and whether arteriogenesis actually results in increased NBF. We tested our hypothesis in vivo by assessing arteriolar density and NBF several days after ultrasound-microbubble treatment.

Methods

Ultrasound Application

The present study was approved by the Animal Research Committee at the University of Virginia and conformed to the American Heart Association guidelines for use of animals in research. Five treatments were applied to the gracilis muscles of 58 Sprague-Dawley rats (Hilltop, Scottdale, Pa) as described in Table 1. Animals were anesthetized by an intraperitoneal injection of ketamine (80 mg/kg) and xylazine (8 mg/kg). The surgical intervention consisted of cannulating the left jugular vein and reflecting the skin back over each gracilis muscle under sterile conditions. Microbubbles (0.4 mL

Received March 29, 2002; revision received June 19, 2002; accepted June 25, 2002.

From the Department of Biomedical Engineering (J.S., M.Q., S.K., R.J.P.) and the Cardiovascular Division (S.K.), University of Virginia, Charlottesville.

Correspondence to Richard J. Price, PhD, Department of Biomedical Engineering, University of Virginia, Box 800759, UVA Health System, Charlottesville, VA 22908. E-mail rprice@virginia.edu

Circulation **is available at http://www.circulationaha.org** **DOI: 10.1161/01.CIR.0000028810.33423.95**

TABLE 1. Experimental Treatments

Treatment Group	n	Surgical Intervention	Microbubble Injection	Ultrasound Application
US-MB-SUR	40	+	+	+
MB-SUR	40	+	+	−
US-SUR	12	+	−	+
SUR	12	+	−	−
CON	6	−	−	−

n indicates number of gracilis muscle specimens per group; +, presence of treatment; and −, absence of treatment. MB-SUR and SUR are paired controls for US-MB-SUR and US-SUR, respectively, consisting of specimens from the contralateral side.

of Optison, Mallinkrodt Medical) were injected intravenously. Ultrasound was applied via a 1-MHz cylindrically focused transducer (Panametrics Inc) with a 1.5-in diameter that was aligned with the gracilis muscle with the use of a custom-designed chamber. The input signal to the transducer was generated by a digital waveform generator (Tektronix AFG-310) and amplified by a 55-dB RF power amplifier (model 3100LA, ENI, Inc). Maximum peak negative pressure at the focus of the transducer was measured with a needle hydrophone (model PVDF-Z44-0400, Specialty Engineering Associates) as 0.75 MPa. Ten seconds after microbubble injection, a pulse of ultrasound, consisting of 100 consecutive 1-MHz sinusoids of 1-V peak-to-peak amplitude from the waveform generator, was applied every 5 seconds for 1 minute. The skin over each muscle was closed with absorbent sutures, and the animals were allowed to recover. To illustrate the presence of red blood cells in the interstitial space, muscles from a single animal were immediately harvested, suffusion-fixed in 4% paraformaldehyde in PBS at 4°C for 3 hours, cryosectioned, and stained with hematoxylin and eosin.

Immunochemistry and Data Acquisition

Specimens were assigned for immunochemical staining and analysis as shown in Table 2. After euthanasia, the abdominal aorta was cannulated, and the vena cava was cut to allow washout of blood. Muscles were perfusion-fixed with 4% paraformaldehyde in PBS for 30 minutes at 4°C and cryosectioned. Cryosections were incubated overnight in 1:200 fluorescein isothiocyanate–conjugated monoclonal anti–smooth muscle (SM) α-actin (clone 1A4, Sigma Chemical Co) in PBS at 4°C. The following day, sections were washed in PBS and mounted for microscopic observation.

Because SM α-actin may be expressed by interstitial myofibroblasts during wound healing, we performed an additional procedure to ensure that SM α-actin staining was colocalized with microvessels. This consisted of labeling muscles from ultrasound-microbubble with surgical intervention (US-MB-SUR) treatment and microbubble injection with surgical intervention but no exposure to ultrasound (MB-SUR) groups at day 14 for endothelial cells with BS-I lectin (Sigma). After SM α-actin labeling, these sections were incubated in 20 μg/mL biotinylated BS-I lectin in PBS for 30 minutes and subsequently incubated in 1:1000 CY3-conjugated streptavidin (Jackson Immunoresearch) for 30 minutes.

Two tissue sections from each muscle, 1 representing the medial and 1 representing the lateral region, were analyzed. Sections were visualized with a Nikon TE-300 inverted microscope and a ×20 PlanFluor objective. Digital images of every field of view within each section were acquired by using a Bio-Rad MicroRadiance confocal scanner. SM α-actin–positive microvessel diameters and the number of SM α-actin–positive microvessels per muscle fiber were measured by an observer blinded to the study protocol. Diameters of noncircular vessel cross sections were derived from inner circumferential tracings.

Flow Measurements

Specimens were assigned for NBF measurements as shown in Table 2. Each animal was anesthetized as described above, the gracilis muscle was exposed and superfused with heated (37°C) Ringer's solution, the mesenteric artery was cannulated for blood sample withdrawal, and a cannula for microsphere injection was placed in the carotid artery and advanced to the aortic arch. For hyperemic NBF measurements, 10^{-4} mol/L adenosine was dissolved in the Ringer's suffusion solution and administered to the muscle. NBF measurements were made by using techniques described in detail elsewhere.[17,18] Briefly, 1.5 mL of 15-μm red fluorescent microspheres (Molecular Probes) was injected into the carotid artery, followed by a 0.25-mL saline flush. Blood collection from the mesenteric artery began simultaneously with microsphere injection and continued for an additional 60 seconds. After euthanasia, gracilis muscles and the blood sample were weighed and chemically digested for 48 hours in 7 mL of 2 mol/L ethanolic KOH containing a known quantity of 15-μm yellow-green microspheres that were added to account for microsphere loss during tissue processing. The same quantity of yellow-green microspheres was used to make a reference sample for estimating the loss of red fluorescence during blood and tissue processing. All samples were then rinsed in 1% Triton X-100 in 10 μmol/L PBS. Microspheres were extracted and subsequently dissolved in 2-ethoxyethyl acetate for 24 hours. A PTI M-2004 fluorimeter (Photon Technology) was used to measure red and yellow-green fluorescence intensities. NBF (mL/min per gram) was determined by using the following equation:

$$NBF = \frac{f_{TR}\left(f_{TYG}/f_{RYG}\right)}{f_{BR}\left(f_{BYG}/f_{RYG}\right)}\frac{R}{M}$$

where f_{TR} is tissue sample red fluorescence, f_{TYG} is tissue sample yellow-green fluorescence, f_{RYG} is reference sample yellow-green fluorescence, f_{BR} is blood sample red fluorescence, f_{BYG} is blood sample yellow-green fluorescence, R is blood sample flow (mL/min), and M is tissue mass (g).

Statistical Analysis

Arterioles per muscle fiber and arteriolar diameters from US-MB-SUR and MB-SUR treatment were analyzed by 2-way repeated-

TABLE 2. Assignment of Specimens for Immunochemistry Procedures or Flow Measurements

	Immunohistochemical Staining					Flow Measurements		
Treatment	Total	Day 3	Day 7	Day 14	Day 28	Total	Hyperemia	Normal Tone
US-MB-SUR	28	6	8	8	6	12	6	6
MB-SUR	28	6	8	8	6	12	6	6
US-SUR	6	0	0	6	0	6	6	0
SUR	6	0	0	6	0	6	6	0
CON	6	0	0	0	0	0	0	0

Numbers in table refer to quantity of gracilis muscle specimens taken for each type of analysis.

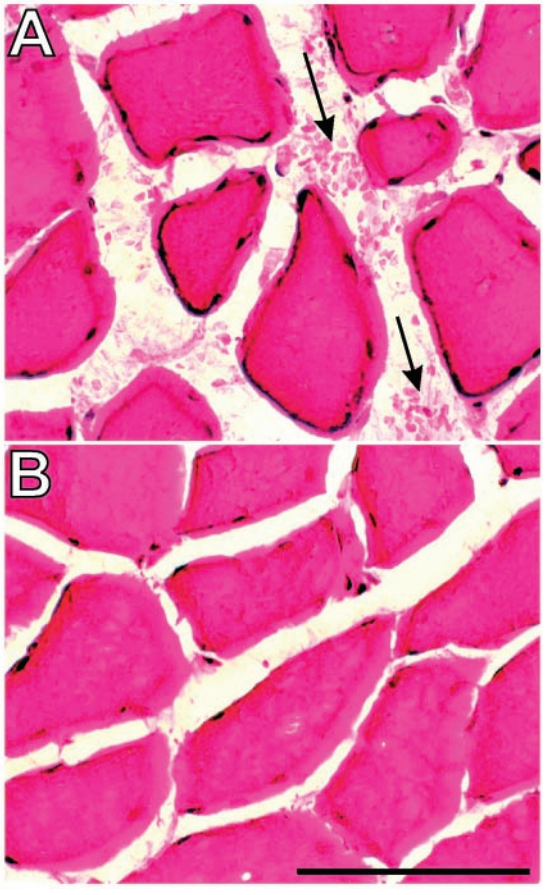

Figure 1. A, Photomicrograph illustrating presence of red blood cells in hematoxylin and eosin (H&E)-stained muscle immediately after US-MB-SUR treatment. Interstitial regions containing extravasated red blood cells (RBCs) are depicted with arrows. B, Contralateral H&E-stained sham (MB-SUR) muscle section after treatment. Note absence of interstitial RBCs with MB-SUR treatment. Bar=100 μm.

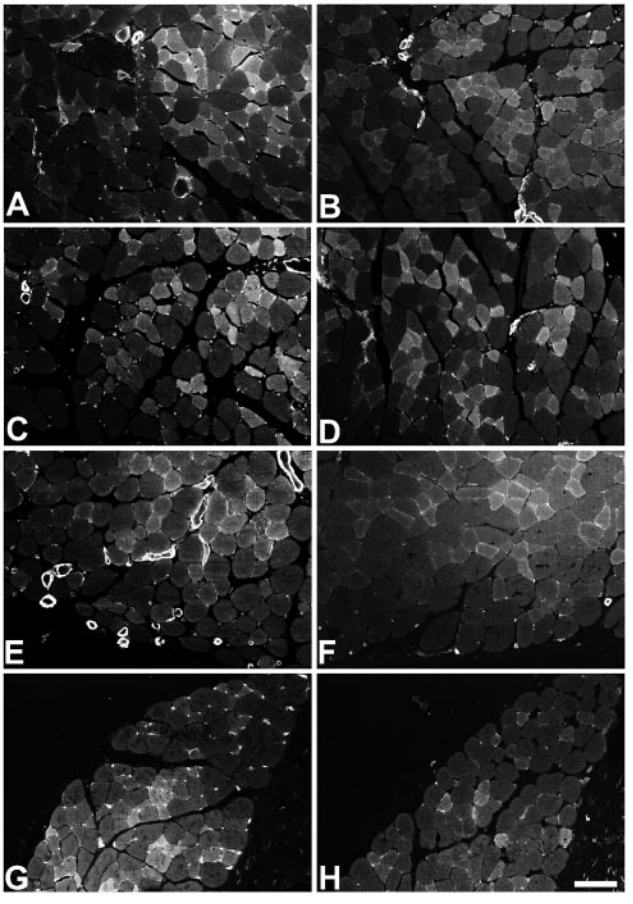

Figure 2. Confocal images of SM α-actin–labeled microvessels in muscles exposed to US-MB-SUR treatment (A, C, E, and G) and sham (MB-SUR) treatment (B, D, F, and H). Images were taken from muscles at 3 (A and B), 7 (C and D), 14 (E and F), and 28 (G and H) days after treatment. SM α-actin–positive microvessels are seen as white dots and circles between muscle fibers, which are visible by autofluorescence. Note apparent increase in number of SM α-actin microvessels at all time points with US-MB-SUR treatment. Bar=100 μm.

measures ANOVA followed by pairwise comparisons with Tukey *t* tests. US-MB-SUR and MB-SUR treatments were compared with treatment with ultrasound plus surgical intervention (US-SUR), treatment with surgical intervention alone (SUR), and no treatment (control [CON]) by using Student *t* tests. NBF data were compared by using paired Student *t* tests. Significance was assessed at $P<0.05$.

Results

Figure 1 illustrates that red blood cells are present in gracilis muscle interstitium immediately after US-MB-SUR treatment (panel A) but are lacking after MB-SUR treatment (panel B). Figure 2 depicts representative muscle sections at 3, 7, 14, and 28 days after US-MB-SUR and MB-SUR treatments. SM α-actin–positive vessels are the white dots and circles between muscle fibers. An increase in SM α-actin–positive vessels is apparent at each time point in US-MB-SUR–treated sections compared with MB-SUR–treated sections. Quantification of this result is presented in Figure 3, which indicates that an $\approx$65% increase in arterioles per muscle fiber occurs at 7 and 14 days in the US-MB-SUR group compared with the MB-SUR group. Furthermore, the numbers of arterioles per muscle fiber are increased at 14 and 28 days in the US-MB-SUR group compared with the CON group. No significant differences in arterioles per fiber were observed between the MB-SUR and CON groups. Moreover, at day 14, US-SUR muscles and their contralateral shams (SUR muscles) exhibited no changes compared with MB-SUR and CON muscles.

Figure 4 illustrates the complete colocalization of SM α-actin–expressing cells with BS-I lectin–labeled microvessels in US-MB-SUR (panel A), MB-SUR (panel B), and CON (panel C) muscles. It is evident that SM α-actin–positive microvessel counts were not skewed by SM α-actin–expressing interstitial cells. Figure 4 also illustrates that microvessel diameters appear to be increased considerably in US-MB-SUR muscles compared with MB-SUR and CON muscles. This observation is quantified in Figure 5, in which arteriolar diameter distributions are presented for the 7- and 14-day groups. At both 7 and 14 days after treatment, compared with MB-SUR values, the numbers of arterioles per fiber were significantly increased in all 4 diameter categories. According to our qualitative observations of these specimens, the majority of the increase in the $>$27-μm grouping was due to the addition of $\approx$30- to 40-μm-diameter arterioles.

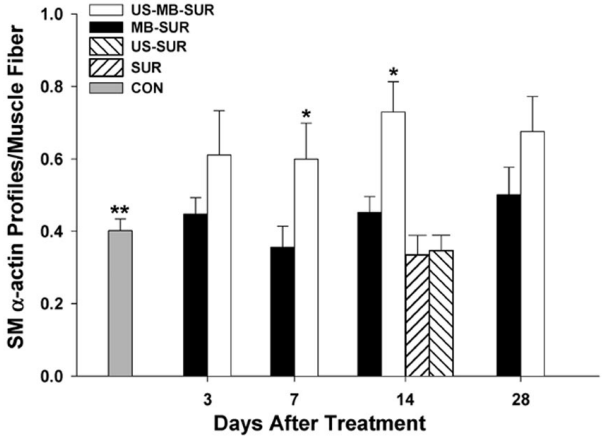

Figure 3. Bar graph showing numbers of arterioles per muscle fiber in muscles exposed to all treatments. Values are mean±SEM. *$P<0.05$ vs MB-SUR for same time point; **$P<0.05$ vs ultrasound-microbubble US-MB-SUR groups at 14 and 28 days ($P<0.05$).

Figure 6 illustrates that these changes in arterioles per muscle fiber and arteriolar caliber result in an increase in NBF 2 weeks after US-MB-SUR treatment. Under conditions of normal tone (Figure 6A), NBF was increased by ≈45% over MB-SUR, but this result is significant only at $P<0.08$. Under conditions of maximum vasodilation, a significant 57% increase in NBF over MB-SUR was observed. Maximal NBF values after US-SUR and SUR treatments were identical to values after MB-SUR treatment.

Discussion

The major finding of the present study is that capillary rupturing elicited by the destruction of ultrasonic contrast agent microbubbles with 1-MHz ultrasound stimulates arteriolar remodeling in skeletal muscle. This response consists of both the formation of new arterioles, which presumably occurs when preexisting capillaries acquire an SM coating, and an increase in the diameter of these newly formed and/or preexisting arterioles into channels with larger diameters. Importantly, this remodeling response creates an increase in hyperemia NBF 2 weeks after treatment, thereby supporting the potential of this technique for restoring NBF to ischemic muscle. Additionally, the inability of 1-MHz ultrasound alone to stimulate arteriolar remodeling or an increase in maximal NBF indicates that microbubbles are required for this response.

We examined the formation and remodeling of microvessels with SM coverage because this process, termed arteriogenesis,[19] may be the preferred mode of revascularization for the relief of ischemia caused by occlusive vascular disease.[20] Compared with capillaries, which form by sprouting during angiogenesis, arteriolar channels better facilitate network resistance reduction and homogeneous blood flow distribution.[20] Arteriogenesis is often studied with the use of angiography, making comparisons with our results from sectioned muscle difficult. However, data acquired in other studies using microangiography, which allows for observations of arterioles as small as ≈30 μm in diameter,[21] can be reasonably compared with data from the >27-μm-diameter group in the present study. Two recent studies have observed arteriogenesis by microangiography in the hindlimb.[21,22] Specifically, ≈2-fold increases in arteriole density were observed for interleukin-10–transfected mice[22] and vascular endothelial

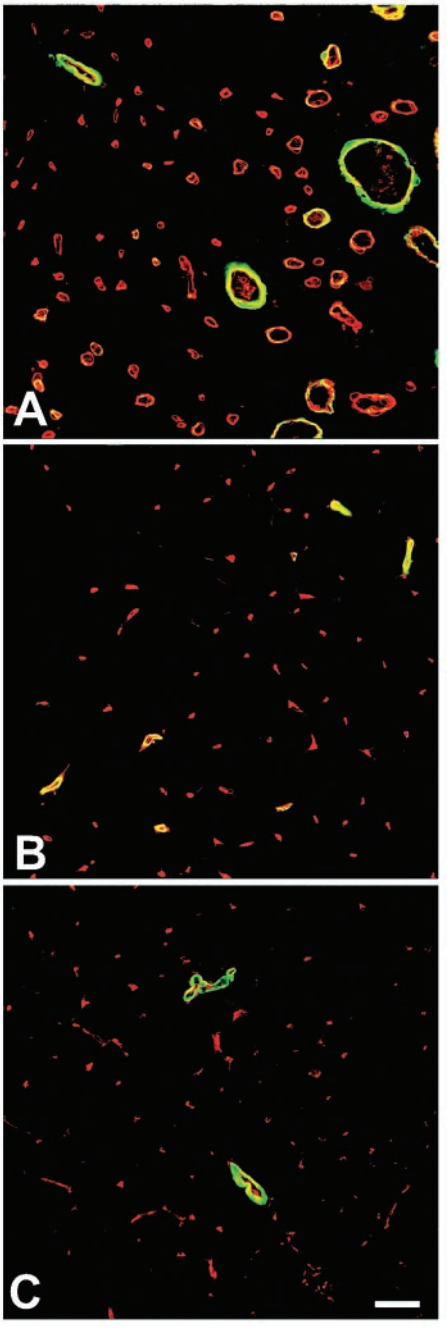

Figure 4. Confocal micrographs illustrating expression of SM α-actin (green fluorescence) in relation to microvessels, as labeled with BS-I lectin (red fluorescence). Images were taken 14 days after muscles were exposed to US-MB-SUR treatment (A), sham (MB-SUR) treatment (B), and CON treatment (C). Note that SM α-actin is colocalized with microvessels, indicating that SM α-actin–positive interstitial myofibroblasts were not present or detectable. Thus, the potential for false-positive arteriolar staining by myofibroblasts was eliminated. Also note that vessel diameters increased significantly with US-MB-SUR treatment compared with MB-SUR and CON treatment. Diameter data are shown in Figure 5. Bar=30 μm.

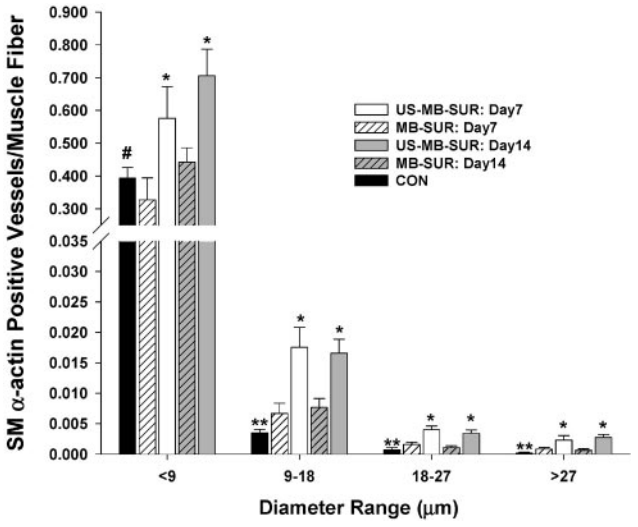

Figure 5. SM α-actin–positive microvessel diameter distributions from US-MB-SUR–treated and sham (MB-SUR)–treated muscles 7 and 14 days after treatment. Untreated CON muscles are also included for comparison. Values are mean±SEM. *$P<0.05$ vs MB-SUR in same diameter category at same time point; **$P<0.05$ vs 7- and 14-day US-MB-SUR groups in same diameter category; and #$P<0.05$ vs 14-day US-MB-SUR group in same diameter category.

growth factor–treated rats subjected to hindlimb ischemia.[21] Although it is likely that it would be difficult to detect by microangiography the 30- to 40-μm-diameter vessels that predominantly account for the large increase seen in the present study and although arteriole density and arterioles per fiber are not equivalent metrics, these studies do support our result that arterioles of this size are capable of considerable remodeling and demonstrate that the response generated by the ultrasound-microbubble technique is comparable to that generated by other experimental stimuli. Clearly, future studies should focus on how the ultrasound-microbubble method influences the remodeling and function of arteriolar channels with larger diameters.

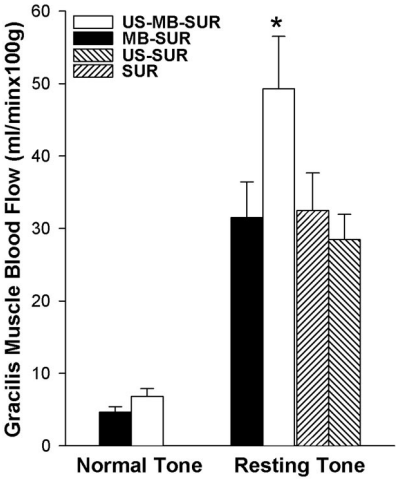

Figure 6. Bar graph of gracilis muscle blood flows under conditions of normal and resting tone 14 days after treatment. Normal tone measurements were made for US-MB-SUR treatment and sham (MB-SUR) treatment. Resting tone measurements were made for US-MB-SUR, MB-SUR, US-SUR, and SUR treatments. Values are mean±SEM. *$P<0.05$ vs MB-SUR.

Under conditions of normal tone, we measured baseline gracilis muscle NBF in sham-treated muscles as 4.6 mL/min per 100 g, a value that agrees well with normal gracilis muscle blood flow measurements made by other investigators (3.3 mL/min per 100 g,[23] 5.6 mL/min per 100 g,[24] and 6.6 mL/min per 100 g[25]), thereby validating our flow measurements and supporting our conclusion that the sham treatment elicits no changes. We observed a trend ($P<0.08$) toward increased NBF in the US-MB-SUR group compared with the contralateral sham control (MB-SUR) group under conditions of normal tone. This result could be attributed to structural remodeling of the vascular network, short-term reductions in local vascular tone, or both. Because of this ambiguity, we also measured NBF under conditions of maximum vasodilation to isolate the contribution of structural remodeling to NBF enhancement. Importantly, 2 weeks after US-MB-SUR treatment, maximum gracilis muscle NBF was markedly increased over MB-SUR treatment. This finding is relevant to the clinical setting in which exercise-induced ischemia is a major problem.

Although we postulate that inflammation created by the rupturing of capillaries initiated the arteriogenesis response, the exact mechanism by which arteriogenesis is stimulated remains to be determined. The creation of capillary ruptures elicits changes in local tissue oxygenation, vasodilation, wall shear stress, and circumferential wall stress, as well as the availability of circulating growth factors to the tissue. Any of these factors could subsequently initiate and maintain the process of arteriogenesis. Moreover, although our results indicate that microbubbles are required for generating the arteriogenesis response, a requirement for capillary rupturing is uncertain. Independent of capillary rupturing, it is possible that thermal, shock-wave, and sonoporation effects could have sheared cell membranes and impacted cell adhesion. With regard to inflammation as a potential stimulus, the linkage between inflammation and arteriogenesis has been solidified at the molecular level in recent studies. It has been shown that collateral vessel formation in the ischemic hindlimb may be stimulated by systemically injecting monocyte chemoattractant protein-1[26,27] or by enhancing monocyte recruitment[28] via lipopolysaccharide administration. Given these results, it is reasonable to postulate that monocyte accumulation after microbubble destruction elicits the remodeling of neighboring arterioles; however, further experimentation is clearly required to address this potential mechanism. Furthermore, the relationship between the degree of inflammation and the extent of remodeling needs to be explored.

Limitations of the Study

Our results suggest that microbubble destruction with ultrasound holds promise as a means for alleviating ischemia in tissue that is compromised by occlusive vascular disease. However, it is important to emphasize that the ultrasound-microbubble treatment was applied to normal hindlimbs, not ischemic hindlimbs. By eliminating the surgical procedure required to produce ischemia, we reduced the number of control groups and removed a number of other confounding

angiogenic factors associated with additional surgery. Although this strategy allowed us to simplify the study, one consequence may have been that the elicited response was transient in nature. Because baseline arteriolar networks provide adequate blood supply to normal skeletal muscle, it is possible that vessel regression began after the initial arteriogenic stimulus had subsided and blood supply was exceeding metabolic demand. To some extent, the data in Figure 3 support this hypothesis because after an increase from 0 to 14 days, the number of arterioles per muscle fiber appears to decrease by day 28. Including a time point beyond 28 days could establish whether the network is returning to baseline; however, it would have little bearing on the clinical feasibility of the method, which must be tested in an ischemic hindlimb model. Indeed, such studies will be needed to determine whether both resting and exercise-induced ischemia can be ameliorated in muscles affected by upstream vascular occlusion. The finding that hyperemia rather than resting NBF was favorably affected also suggests that arteriogenesis in the nonischemic muscle may enhance exercise-induced performance.

Finally, we emphasize that in the present study, capillary rupturing was generated with ultrasound at a subclinical frequency of 1 MHz. At clinical frequencies (>2.2 MHz), the ability of ultrasound-microbubble interactions to create capillary rupturing and hemorrhage is controversial. Capillary rupturing in intact mouse skeletal muscle with clinical ultrasound has been demonstrated.[15] However, in our laboratory, the interaction of 2.3-MHz ultrasound with microbubbles creates capillary rupturing only in exteriorized skeletal muscle, where tissue attenuation of ultrasound power is minimal. To generate capillary rupturing in intact rat muscle, we found that it was necessary to lower the frequency to 1 MHz. The disruption of capillary endothelium and underlying basement membrane by 1-MHz ultrasound in the presence of microbubbles has also been documented by others.[29,30]

Acknowledgments

Dr Song was the recipient of a postdoctoral fellowship grant from the American Heart Association Mid-Atlantic Affiliate, Baltimore, Md. Dr Kaul was supported by grants from the National Institutes of Health, Bethesda, Md (RO1 HL-48890 and RO1 HL-65704). Dr Price was supported by grants from the Whitaker Foundation, Rosslyn, Va (RG980402), the American Heart Association, Dallas, Tex (9730025N), and the National Institutes of Health, Bethesda, Md (RO1 HL-66307).

References

1. Losordo DW, Vale PR, Isner JM. Gene therapy for myocardial angiogenesis. *Am Heart J*. 1999;138:S132–S141.
2. Rosengart TK, Patel SR, Crystal RG. Therapeutic angiogenesis: protein and gene delivery strategies. *J Cardiovasc Risk*. 1999;6:29–40.
3. Tomanek RJ, Schatteman GC. Angiogenesis: new insights and therapeutic potential. *Anat Rec*. 2000;261:126–135.
4. Webster RA. Therapeutic angiogenesis: a case for targeted, regulated gene delivery. *Crit Rev Eukaryot Gene Expr*. 2000;10:113–125.
5. Bortone AS, D'Agostino D, Schena S, et al. Inflammatory response and angiogenesis after percutaneous transmyocardial revascularization. *Ann Thorac Surg*. 2000;70:1134–1138.
6. Malekan R, Reynolds C, Narula N, et al. Angiogenesis in transmyocardial revascularization: a nonspecific response to injury. *Circulation*. 1998; 98(suppl II):II-62–II-65.
7. Roethy W, Yamamoto N, Burkhoff D. An examination of potential mechanisms underlying transmyocardial laser revascularization induced increases in myocardial blood flow. *Semin Thorac Cardiovasc Surg*. 1999;11:24–28.
8. Victor C, Jin-qiang K, McGInn A, et al. Angiogenic response induced by mechanical transmyocardial revascularization. *J Thorac Cardiovasc Surg*. 199;118:849–856.
9. Mukherjee D, Wong J, Griffin B, et al. Ten-fold augmentation of endothelial uptake of vascular endothelial growth factor with ultrasound after systemic administration. *J Am Coll Cardiol*. 2000;35:1678–1686.
10. Porter TR, Iversen PL, Li S, et al. Interaction of diagnostic ultrasound with synthetic oligonucleotide-labeled perfluorocarbon-exposed sonicated dextrose albumin microbubbles. *J Ultrasound Med*. 1996;15: 577–584.
11. Shohet RV, Chen S, Zhou Y-T, et al. Echocardiographic destruction of albumin microbubbles directs gene delivery to the myocardium. *Circulation*. 2000;101:2554–2556.
12. Price RJ, Skyba DM, Kaul S, et al. Delivery of colloidal particles and red blood cells to tissue through microvessel ruptures created by targeted microbubble destruction with ultrasound. *Circulation*. 1998;98: 1264–1267.
13. Song J, Chappell JC, Qi M, et al. Influence of injection site, microvascular pressure, and ultrasound variables on microbubble-mediated delivery of microspheres to muscle. *J Am Coll Cardiol*. 2002;39: 726–731.
14. Skyba DM, Price RJ, Linka AZ, et al. Direct in vivo visualization of intravascular destruction of microbubbles by ultrasound and its local effects on tissue. *Circulation*. 1998;98:290–293.
15. Miller DL, Quddus J. Diagnostic ultrasound activation of contrast agent gas bodies induces capillary rupture in mice. *Proc Natl Acad Sci U S A*. 2000;97:10179–10184.
16. Ay T, Havaux X, Van Camp G, et al. Destruction of microbubbles by ultrasound: effects on myocardial function, coronary perfusion pressure, and microvascular integrity. *Circulation*. 2001;104:461–466.
17. Glenny RW, Bernard S, Brinkley M. Validation of fluorescent-labeled microspheres for measurement of regional organ perfusion. *J Appl Physiol*. 1993;74:2585–2597.
18. Unthank JL, Nixon JC, Burkhart HM, et al. Early collateral and microvascular adaptations to intestinal artery occlusion in rat. *Am J Physiol*. 1996;270:H914–H923.
19. Buschmann I, Schaper W. The pathophysiology of the collateral circulation (arteriogenesis). *J Pathol*. 2000;190:338–342.
20. Simons M, Bonow R, Chronos NA, et al. Clinical trials in coronary angiogenesis: issues, problems, consensus. *Circulation*. 2000;102: e73–e86.
21. Takeshita S, Isshiki T, Ochiai M, et al. Endothelium-dependent relaxation of collateral microvessels after intramuscular gene transfer of vascular endothelial growth factor in a rat model of hindlimb ischemia. *Circulation*. 1998;98:1261–1263.
22. Silvestre J-S, Mallat Z, Duriez M, et al. Antiangiogenic effect of interleukin-10 in ischemia-induced angiogenesis in mice hindlimb. *Circ Res*. 2000;87:448–452.
23. Heinrich HN, Hecke A. A gracilis muscle preparation for quantitative microcirculatory studies in the rat. *Microvasc Res*. 1978;15:349–356.
24. Honig CR. Hypoxia in skeletal muscle at rest and during the transition to steady work. *Microvasc Res*. 1977;13:377–398.
25. Honig CR, Frierson JL, Patterson JL. Comparison of neural controls of resistance and capillary density in resting muscle. *Am J Physiol*. 1970; 218:937–942.
26. Ito WD, Arras M, Winkler B, et al. Monocyte chemoattractant protein-1 increases collateral and peripheral conductance after femoral artery occlusion. *Circ Res*. 1997;80:829–837.
27. Scholz D, Ito W, Fleming I, et al. Ultrastructure and molecular histology of rabbit hind-limb collateral artery growth (arteriogenesis). *Virchows Arch*. 2000;436:257–270.
28. Arras M, Ito WD, Scholz D, et al. Monocyte activation in angiogenesis and collateral growth in the rabbit hindlimb. *J Clin Invest*. 1998;101: 40–50.
29. Miller DL, Gies RA. Gas-body-based contrast agent enhances vascular bioeffects of 1.09 MHz ultrasound on mouse intestine. *Ultrasound Med Biol*. 1998;24:1201–1208.
30. Miller DL, Gies RA. The influence of ultrasound frequency and gas-body composition on the contrast agent-mediated enhancement of vascular bioeffects in mouse intestine. *Ultrasound Med Biol*. 2000;26:307–313.